JOURNAL OF MATERIALS SCIENCE 6 (1971) 989–997

Kinetics and Mechanisms of Pore Growth in MgO

TAPAN K. GUPTA
Ceramics & Glasses, Westinghouse Research Laboratories, Pittsburgh, Pennsylvania 15235, USA

Isothermal pore growth occurs in MgO when polycrystalline compacts are annealed in air for long periods of time at temperatures between 1450 and 1650°C. Fractographic examination of the microstructures demonstrates that the pores are trapped along the grain boundaries and at the intersections. The growth occurs as a result of pore dragging by grain boundary in combination with transport of atoms by surface diffusion. The contribution from lattice diffusion and vapour transport becomes increasingly important as the temperature is raised. Finally, as the pores grow in size, they inhibit the normal grain growth in MgO.

1. Introduction

The phenomenon of pore migration or bubble migration in solids was first demonstrated by Barnes and Mazey [1] in thin copper foils and was subsequently observed in other metal [2–5] and oxide [6–7] systems. The first theoretical treatment of pore migration was given by Shewmon [8] who generated a series of equations for cases of various transport mechanisms under an imposed driving force. According to Nichols [9], the imposed driving forces include: thermal gradient, bowed dislocation, curved grain boundary, and electrical potential gradient. Examples of pore migration under a strong thermal gradient are those in copper [1] as cited above and in UO_2 thin foils [5], as observed in the electron microscope by using a pulse annealing technique. Pores and bubbles are also known to migrate when there is no imposed driving force such as the case when migration occurs due to random atomic fluxes under isothermal heating conditions. In one series of experiments, pore migration in solids under isothermal anneal was studied following inert gas bombardment or radiation damage in solids [3, 4, 6]. In an entirely different series of studies, pore migration and coalescence were observed during sintering of a number of polycrystalline materials in air or in inert atmospheres. Examples are: pore growth in Cu [10–12], UO_2 [13], ZnO [14], and MgO [15]. During the last stage of sintering, a fraction of the pores containing insoluble gases is normally trapped in the solid. As the pores shrink in size, the gas pressure in the pore (ΔP increases, until it equilibrates with the surface energy (γ_{sv}) according to the relation $\Delta P = 2\gamma_{sv}/r$, where r is the radius of the pore. Upon further heating, the pores grow in size and decrease in number as the diffusion of the gas to the surface becomes negligible compared to the diffusion flux between the pores [14]. In a polycrystalline material, the pores can also be dragged by the boundaries when they are located on the plane of grain boundaries and finally coalesce. This possibility was first suggested by Kingery and Francois [21] and following that argument, Nichols [22] subsequently explained the grain growth kinetics in UO_2. More recently, Brook [32] has discussed the conditions under which the interaction of pore and grain boundary may occur.

Analysis of pore migration by diffusion control mechanism has been made by a number of authors [8–10, 12–14, 17–20]. Nichols has recently reviewed the kinetics for various driving forces [9]. The possible rate controlling mechanisms discussed are: surface diffusion, lattice diffusion and vapour transport. In the absence of an imposed driving force, the pore diffusion coefficient (defined as the pore mobility times kT, where kT is the usual thermal energy) for each of these mechanisms has been shown to vary as D_s/d^4, D_L/d^3 and D_g/d^3, respectively, where d is the pore diameter and D_s, D_L and D_g are the surface diffusion coefficient, lattice diffusion coefficient and diffusion coefficient in

the gas respectively and where D_g may depend on d. Typically, surface diffusion dominates for submicron sizes followed by volume diffusion or vapour transport for sizes in the range of few to 10 μm. The dominant mechanism is determined by comparing the velocities predicted for these mechanisms with those observed experimentally.

In the analysis that follows, the pore growth kinetics in polycrystalline MgO during the late stage of sintering (when the specimens are partially or completely impervious) are analysed following the mechanisms of material transport as delineated above. Pore velocities are estimated according to each mechanism from a knowledge of atomic parameters and compared with the experimental velocities. The rate controlling mechanism is then determined by a process of elimination. Accounts are taken of the possible effect of grain growth on the pore growth kinetics in MgO.

2. Experimental Procedure

The magnesium oxide powder, obtained by calcination of hydroxide, was isostatically pressed at 21×10^6 kgs/m^{-2} and annealed between 1450 and 1650°C for extended periods of time. The powder characteristics and the details of heat treatment were reported elsewhere [25]. The specimens used in the present investigation had a bulk density between 90 and 98% of the theoretical and they exhibited partial to complete imperviousness. Normally. an expansion of the specimens was observed at a given temperature when annealed for a long period of time.

Preliminary examination of the microstructure indicated that a large number of pores were trapped along the grain boundaries and at boundary intersections. In order to estimate the size of these pores, the specimens were then treated for fractographic analysis in the electron microscope. The freshly fractured surface of MgO was coated with a heavy layer of carbon which was then floated off the samples by immersing in 1:1 dilute nitric acid for 2 to 5 min. The replica thus obtained was then examined in the electron microscope after proper cleaning. Since the fracture was primarily occurring in an intergranular fashion, the pores which were located on the plane of grain boundaries could be easily identified from the examination of the fractographs. They were then measured by a calibrated magnifying eye-piece placed directly over the fractographs. The smallest size that could be measured this way was of the order of ~ 0.2 μm. The number of counts made at a given temperature and time normally ranged from 50 to 100 or more, depending on the nature of fractographs. Special attention was directed to measuring those pores which were spherical in shape and lying directly in the plane of the grain boundary. With elliptical pores, both major and minor axes were determined and the average of the two was reported as the estimated pore diameter. The possible error that can enter into pore measurement came primarily from the variation of electron beam during examination of the replica, and was estimated to be in the range of $\pm$ 10%.

The grain size was measured from the optical microstructures developed from the polished section of MgO by counting the number of grain boundaries intersected by measured lengths of random straight lines drawn directly on photomicrographs. The grain size reported was 1.5 times the average intercept lengths thus obtained by lineal analysis.

3. Experimental Data and Calculation

Fig. 1 illustrates the typical fractographs from which the pore sizes were measured. The pores which were located only on the plane of grain boundary and are not intersected by the lines, were counted for the frequency-size distribution as shown for a typical distribution in fig. 2. Average pore diameters were calculated from such distributions. Pertinent data regarding experimental temperature, annealing time, average pore diameter and grain size are listed in the first four columns of table I. The number of pores per unit volume, N_V (number/cm^3), was calculated from a knowledge of fractional pore volume (V) and the pore diameter (d) through the relation:

$$V = N_V \frac{\pi}{6} d^3 \qquad (1)$$

and is reported in column 5 of table I. The grain boundary area per unit volume A_V (cm^2/cm^3) was estimated from the photomicrographs by counting the number of grains traversed per cm (N_L) by a random line using the relation [26, 27]:

$$A_V = 2N_L \qquad (2)$$

and is listed in column 6 of table I. By using the above two relations the total number of pores per unit area of grain boundary, N_{gb} (number/cm^2 of grain boundary) is calculated in column 7. The final column gives an estimate of pore-to-

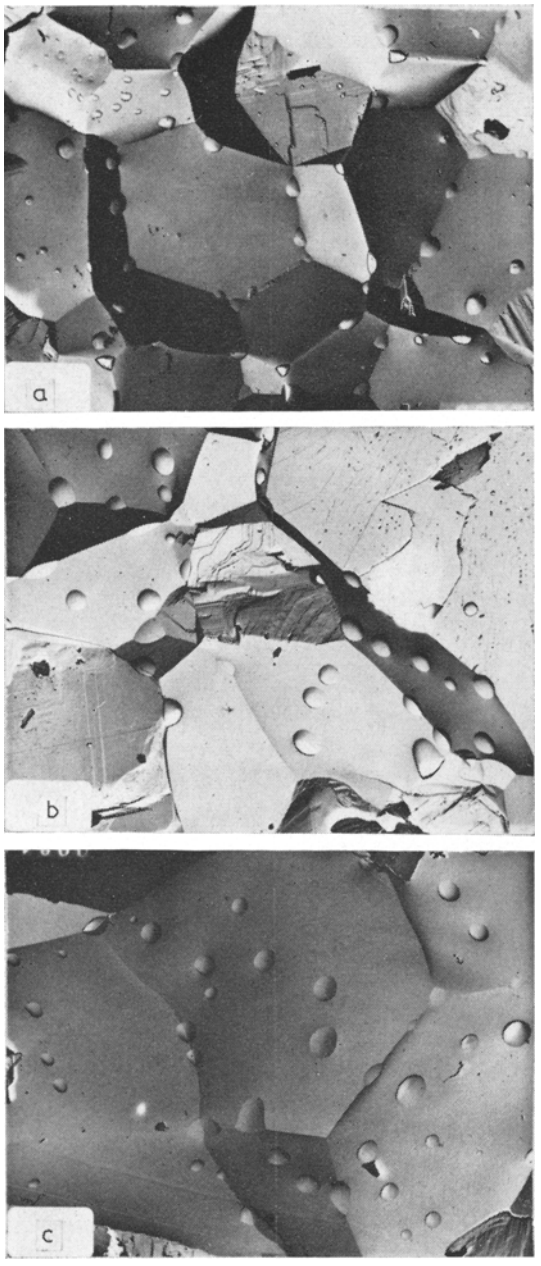

Figure 1 Fractured surfaces of MgO annealed at 1650° C for (a) 100, (b) 500 and (c) 1000 min, respectively (× 2700).

pore spacings, l (cm), calculated from the relation:

$$l = \frac{1}{\sqrt{N_{gb}}} \qquad (3)$$

It is seen from table I that the pore size and grain size continuously increase with time at a given annealing temperature. Using the appropriate time exponent as discussed later, it can be shown that the pore size at each temperature can be extrapolated to zero co-ordinate thus satisfying the boundary conditions: size = 0 at time = 0. These conditions are used during subsequent calculation of pore velocities.

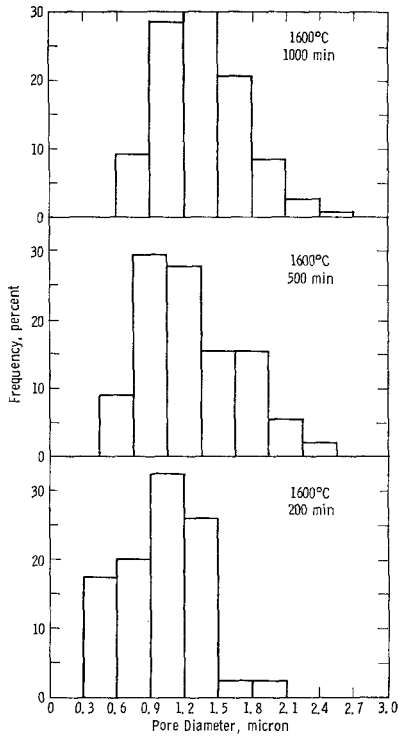

Figure 2 Typical histograms of the grain boundary pores in polycrystalline MgO at 1600° C and for various annealing times.

Corresponding to the observation that the pore size increases with annealing time, the number of pores per unit volume N_V is seen to decrease with increased annealing time except in few instances with long annealing times and at higher temperatures. This discrepancy may have resulted from the averaging of pore diameters necessary for such calculation. The greatest amount of uncertainty arises in the estimates of the number of pores per unit area of the grain boundary, N_{gb} and the pore-to-pore spacing, l. Here the primary source of inaccuracy comes from the measurement of the grain boundary area per unit volume, which depends on the accurate determination of the intercept length of the representative grain structures. Based on the above limitation, the general observation is that

TABLE I Pertinent data on pore growth in polycrystalline MgO between 1450 and 1650° C for various annealing times

Temperature °C	Time min.	Average pore diameter (d) (μm)	Average grain size (g) (μm)	Number of pores number/cm^3 (N_v)	Grain boundary area cm^2/cm^3 (A_v)	Number of pores Number/cm^2 (N_{gb})	Pore spacings $l = 1/\sqrt{N_{gb}}$ (cm)
1650	1000	1.41	30.0	4.9×10^{10}	1.00×10^3	4.90×10^7	1.43×10^{-4}
	500	1.25	24.7	7.1×10^{10}	1.21×10^3	5.80×10^7	1.31×10^{-4}
	200	1.23	23.1	5.3×10^{10}	1.30×10^3	4.08×10^7	1.56×10^{-4}
	100	0.899	20.2	2.1×10^{11}	1.48×10^3	1.42×10^8	8.40×10^{-5}
	60	0.791	18.5	3.9×10^{11}	1.63×10^3	2.39×10^8	6.45×10^{-5}
	30	0.628	18.1	4.1×10^{11}	1.67×10^3	2.46×10^8	6.37×10^{-5}
1600	1000	1.33	33.8	5.6×10^{10}	8.93×10^2	6.28×10^7	1.26×10^{-4}
	500	1.22	30.9	1.7×10^{10}	9.71×10^2	1.75×10^7	2.39×10^{-4}
	200	0.997	25.3	1.4×10^{11}	1.18×10^3	1.19×10^8	9.17×10^{-5}
	50	0.599	13.0	2.8×10^{11}	2.31×10^3	1.21×10^8	9.09×10^{-5}
1550	1000	1.27	28.2	4.7×10^{10}	1.06×10^3	4.44×10^7	1.50×10^{-4}
	500	1.05	25.9	1.1×10^{11}	1.16×10^3	9.50×10^7	1.03×10^{-4}
	200	0.849	21.6	1.9×10^{11}	1.39×10^3	1.37×10^8	8.55×10^{-5}
	30	0.564	9.1	7.8×10^{11}	3.30×10^3	2.36×10^8	6.54×10^{-5}
1500	1000	1.06	31.8	9.7×10^{10}	9.43×10^2	1.03×10^8	9.90×10^{-5}
	500	0.940	27.3	4.0×10^{11}	1.09×10^3	3.68×10^8	5.21×10^{-5}
	100	0.688	10.5	5.6×10^{11}	2.86×10^3	1.96×10^8	7.14×10^{-5}
1450	1000	1.03	30.8	1.2×10^{11}	9.70×10^2	1.24×10^8	9.01×10^{-5}
	450	0.86	19.7	1.8×10^{11}	1.53×10^3	1.18×10^8	9.17×10^{-5}

the number of pores per unit area of the grain boundary, N_{gb}, seems to increase and the pore-to-pore spacing, l, seems to decrease with the increase in the grain boundary area or with the decrease in the pore size.

4. Comparison of the Experimental Data with Calculated Values

4.1. Estimation of D_p from Experimental Data

The pore diffusion coefficient, D_p, for an assembly of pores executing a random motion in the plane of grain boundary can be obtained from Fick's law of diffusion. The two-dimensional mean square distance x^2 travelled by a pore with no driving force in time t is given by:

$$x^2 = 4D_p t \tag{4}$$

Following Wolfenden and Farrell [24] the value of x can be obtained from a knowledge of the probability of a pore moving in a straight line and colliding with a second pore at a distance x in the plane of grain boundary:

$$x = \frac{1}{N_{gb}(2d)} \tag{5}$$

where d is the diameter of the pore and N_{gb} is the average pore density on grain boundary, defined by $1/l^2$ where l is the average pore-pore spacings in the grain boundary. Combining the two equations and substituting for N_{gb} gives:

$$D_p = \frac{l^4}{16\theta d^2 t} \tag{6}$$

Thus the pore diffusion coefficient can be calculated from a knowledge of average pore-pore spacing, average pore diameter and the annealing time as listed in table I. Since the mechanism of migration enters only through D_p, the calculated pore diffusion coefficients from the experimental data can be compared directly with those calculated for surface diffusion, lattice diffusion or vapour transport mechanism from atomic parameters. In doing such comparison, it is assumed that the mathematical derivation for pore diffusivities as related to atomic parameters is the same for grain boundaries as for the matrix, but it is noted that the grain boundaries may exert an influence on atomic parameters. It is further assumed that there is no pore migration due to an interface control mechanism as discussed by Herring [28] and Nichols [9]. This assumption is acceptable in view of the fact that the pores are nearly spherical and have no faceting configuration. Finally, it must be pointed out that the single major uncertainty in calculating D_p from equation 6 is introduced through the term l^4, since an error in l will now

TABLE II Comparison of pore diffusivities in MgO calculated from appropriate atomic parameters and those calculated from the experimental data

Temperature °C	Time (min)	Pore diameter (d) (μm)	Experimental D_p (cm²/sec)	Surface diffusion $D_p(s)$ (cm²/sec)	Lattice diffusion $D_p(L)$ (cm²/sec)	Vapour transport $D_{p(V)}$ (cm²/sec)
1650	1000	1.41	2.18×10^{-14}	1.27×10^{-19}	3.92×10^{-21}	5.20×10^{-22}
	500	1.25	3.94×10^{-14}	2.06×10^{-19}	5.64×10^{-21}	7.45×10^{-22}
	200	1.23	2.02×10^{-13}	2.21×10^{-19}	5.90×10^{-21}	7.82×10^{-22}
	100	0.899	6.42×10^{-14}	7.66×10^{-19}	1.51×10^{-20}	2.00×10^{-21}
	60	0.791	4.78×10^{-14}	1.27×10^{-18}	2.22×10^{-20}	2.94×10^{-21}
	30	0.628	1.47×10^{-13}	3.32×10^{-18}	4.45×10^{-20}	5.86×10^{-21}
1600	1000	1.33	1.50×10^{-14}	7.22×10^{-20}	2.62×10^{-21}	2.54×10^{-22}
	500	1.22	4.56×10^{-13}	1.03×10^{-19}	3.30×10^{-21}	3.28×10^{-22}
	200	0.997	3.72×10^{-14}	2.30×10^{-19}	6.20×10^{-20}	6.00×10^{-22}
	50	0.599	3.94×10^{-13}	1.74×10^{-18}	2.86×10^{-20}	2.78×10^{-21}
1550	1000	1.27	3.28×10^{-14}	7.15×10^{-20}	1.81×10^{-21}	1.16×10^{-22}
	500	1.05	2.12×10^{-14}	1.53×10^{-19}	3.20×10^{-21}	2.06×10^{-22}
	200	0.849	3.86×10^{-14}	3.57×10^{-19}	6.06×10^{-21}	3.90×10^{-22}
	30	0.564	1.99×10^{-13}	1.81×10^{-18}	2.07×10^{-20}	1.33×10^{-21}
1500	1000	1.06	8.90×10^{-15}	7.36×10^{-20}	1.60×10^{-21}	8.23×10^{-23}
	500	0.940	1.74×10^{-15}	1.19×10^{-19}	2.29×10^{-21}	1.18×10^{-22}
	100	0.688	5.78×10^{-14}	4.17×10^{-19}	5.84×10^{-21}	3.00×10^{-22}
1450	1000	1.03	6.45×10^{-15}	4.07×10^{-20}	9.17×10^{-22}	3.64×10^{-23}
	450	0.86	2.24×10^{-14}	8.55×10^{-20}	1.57×10^{-21}	6.20×10^{-23}

be magnified to a power of four. In view of all these, it is recognised that a comparison between the estimated and the experimental D values can be made only to the extent of an order of magnitude reliability.

The experimental pore diffusion coefficients as calculated from equation 6 by using the data in table I are shown in table II along with other estimated values from surface, lattice and vapour transport mechanisms respectively. It is seen that the experimental data fall within the range of 10^{-13} to 10^{-15} cm²/sec, the majority having a value of 10^{-14} cm²/sec. A further general observation is that as the temperature is raised or the pore size decreased, the pore diffusion coefficient appears to show a slightly higher value.

4.2. Pore Migration by Surface Diffusion

The pore diffusion coefficient for surface diffusion mechanism is given by [9]:

$$D_{p(s)} = \frac{3 D_s \lambda \Omega}{2\pi (d/2)^4} \qquad (7)$$

where λ = normal spacings in the lattice between diffusing (rate-controlling) species, and Ω = molecular volume of the matrix material. For calculation, it is assumed that $\lambda = 3$ Å, Ω = (mole weight/density × Avogadro's number) = 1.83×10^{-23} cm³, and that the surface diffusion coefficient is isotropic on all grain boundaries. In the absence of a known slower diffusing species for surface diffusion in MgO, the values used for calculation are those obtained by Robertson [29]:

$$D_s = 2.3 \times 10^5 \exp\left[-\frac{90 \text{ kcal}}{RT}\right] \text{cm}^2/\text{sec}$$

Using the above data in conjunction with the average pore diameter in table I, the calculated values of $D_{p(s)}$ are reported in table II. The calculated pore diffusivity $D_{p(s)}$ at all temperatures is seen to be several orders of magnitude smaller than the experimental diffusivities D_p. Had the calculations been deliberately based on the faster surface diffusing species in MgO, the values would be reduced by the selection of the slower diffusing species in MgO. Clearly for the pore sizes involved, the kinetics of migration and coalescence is not controlled by a mechanism of random, two-dimensional migration of pores by surface diffusion mechanism. This observation is further substantiated by the fact that a plot D_p versus d^4 does not yield a straight line, even within the limits of uncertainties.

4.3. Pore Migration by Lattice Diffusion

The pore diffusion coefficient for lattice diffusion

mechanism is given by [9]:

$$D_{p(L)} = \frac{3D_L\,\Omega}{4\pi(d/2)^3} \quad (8)$$

The lattice diffusion coefficient D_L is obtained from that determined by Lindner and Parfitt [30] for magnesium in MgO.

$$D_{Mg\rightarrow MgO} = 0.249 \exp\left[-\frac{79\ \text{kcal}}{RT}\right] \text{cm}^2/\text{sec}$$

The calculated values of pore diffusion coefficients, $D_{p(L)}$ are reported in table II and are found to be smaller by several orders of magnitude than the experimental diffusivities. Using the values for the lattice diffusion of oxygen in MgO as reported by Oishi and Kingery [31], the disagreement between the experimental and calculated diffusivities is further widened, since the oxygen diffusion in MgO is several orders of magnitude lower than the magnesium diffusion in MgO. Furthermore, a plot of D_p versus d^3 does not yield a straight line within the experimental uncertainties. In view of this, the possibility of lattice diffusion as the rate controlling mechanism, assuming random migration and coalescence of the pores, has been ruled out.

4.4. Pore Migration by Vapour Transport

The pore diffusion coefficient for vapour transport mechanism is given by [9]:

$$D_{p(V)} = \frac{3D_g\,\Omega^2\,\alpha_V P_V}{4\pi\,kT(d/2)^3} \quad (9)$$

where P_V is the equilibrium vapour pressure of the rate controlling species and $\alpha_V(\leq 1)$ is a measure of the departure from the equilibrium. The value of P_V for MgO is obtained from the literature [33] and α_V is assumed to have a value equal to 1, bearing in mind that this is the maximum possible value of α_V. A reasonable value of D_g from the kinetic theory of gas [34] is estimated to be 1 cm²/sec with extremes of 0.1 and 10 cm²/sec. Assuming that D_g is independent of temperature within the range of measurement made, the pore diffusivities due to vapour transport are calculated in table II. The results are found to be in wide disagreement with the experimental values. When compared with the pore diffusivities due to surface and lattice diffusion of atoms, vapour transport data give values which are smaller by one to two orders of magnitude. By having lower values of α_V (< 1) and D_g (< 1 cm²/sec) than those assumed in the calculation, pore diffusivities are correspondingly reduced and the disagreement with the experimental results is further widened. By using higher values of D_g ($\simeq 10$ cm²/sec) the conclusion remains essentially unaltered. In view of this, the vapour transport is not considered as a rate controlling mechanism assuming random motion of pores.

4.5. Pore Migration due to Boundary Migration

Since there is a certain amount of grain growth during pore growth as shown in table I, the possibility exists that the pores are dragged by the grain boundaries as grain growth proceeds [21]. The normal grain boundary mobility will therefore be reduced as a result of the presence of the pores on boundaries. Fig. 3 shows the log-log

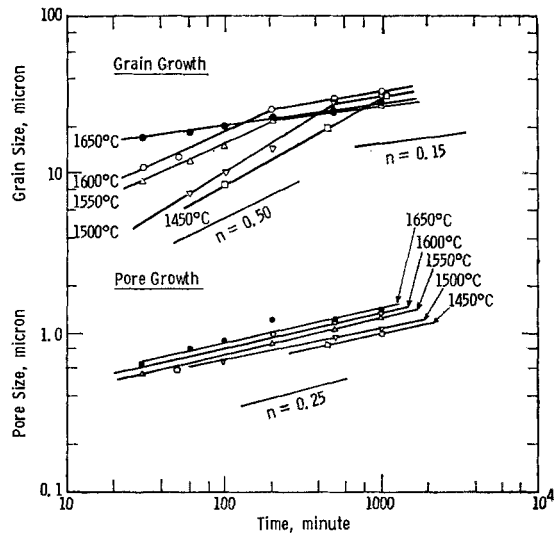

Figure 3 Log-log plot of pore size and grain size versus annealing time in polycrystalline MgO for various annealing temperatures.

plots of the grain size versus time and the pore size versus time for the same specimens. Within the range of experimental data shown, the time dependence of pore growth can be approximated by an exponent equal to $n = 0.25$ while the time dependence for grain growth changes from $n = 0.50$ (which is the time dependence for grain growth during sintering [25]) to $n = 0.15$, the latter exponent clearly reflecting the pronounced dragging effect [35] of porosity on the rate of normal grain growth in MgO. The effect is most pronounced at the highest temperature of measurement and least pronounced at the

TABLE III Pore velocity in MgO: comparison of the experimental data with those estimated from atomic parameters

Temperature °C	Time (min)	Pore diameter (d) (μm)	Experimental pore velocity V_p (cm/sec)	Estimated pore velocity due to boundary migration and Surface diffusion $V_{p(s)}$ (cm/sec)	Lattice diffusion $V_{p(L)}$ (cm/sec)	Vapour transport $V_{p(v)}$ (cm/sec)
1650	1000	1.41	2.35×10^{-9}	4.16×10^{-8}	1.28×10^{-9}	1.71×10^{-10}
	500	1.25	4.17×10^{-9}	6.00×10^{-8}	1.64×10^{-9}	2.17×10^{-10}
	200	1.23	1.02×10^{-8}	6.34×10^{-8}	1.68×10^{-9}	2.24×10^{-10}
	100	0.899	1.50×10^{-8}	1.60×10^{-7}	3.14×10^{-9}	4.17×10^{-10}
	60	0.791	2.20×10^{-8}	2.34×10^{-7}	4.08×10^{-9}	5.41×10^{-10}
	30	0.628	3.50×10^{-8}	4.85×10^{-7}	6.50×10^{-9}	8.58×10^{-10}
1600	1000	1.33	2.22×10^{-9}	2.30×10^{-8}	8.35×10^{-10}	8.10×10^{-11}
	500	1.22	4.07×10^{-9}	3.02×10^{-8}	9.66×10^{-10}	9.56×10^{-11}
	200	0.997	8.30×10^{-9}	5.50×10^{-8}	1.49×10^{-9}	1.44×10^{-10}
	50	0.599	1.98×10^{-8}	2.50×10^{-7}	4.10×10^{-9}	3.98×10^{-10}
1550	1000	1.27	2.11×10^{-9}	2.24×10^{-8}	5.67×10^{-10}	3.63×10^{-11}
	500	1.05	3.50×10^{-9}	3.96×10^{-8}	8.32×10^{-10}	5.34×10^{-11}
	200	0.849	7.06×10^{-9}	7.50×10^{-8}	1.27×10^{-9}	8.15×10^{-11}
	30	0.564	3.13×10^{-8}	2.52×10^{-7}	2.88×10^{-9}	1.85×10^{-10}
1500	1000	1.06	1.77×10^{-9}	1.98×10^{-8}	4.30×10^{-10}	2.21×10^{-11}
	500	0.940	3.14×10^{-9}	2.84×10^{-8}	5.45×10^{-10}	2.80×10^{-11}
	100	0.688	1.15×10^{-8}	7.30×10^{-8}	1.02×10^{-9}	5.25×10^{-11}
1450	1000	1.03	1.72×10^{-9}	1.09×10^{-8}	2.47×10^{-10}	9.75×10^{-12}
	450	0.86	3.18×10^{-9}	1.92×10^{-8}	3.51×10^{-10}	1.39×10^{-11}

lowest temperature of measurement. Apparently, at 1650°C, the pore entrapment occurs within a few minutes of sintering [25] while at 1450°C pore entrapment occurs only after sintering for 1000 min. The result thus indicates that with the pore entrapment at the boundary, the pore velocity controls the grain growth rate in MgO. Had the pore and boundary velocities remained the same, the pores would not have inhibited the grain growth as illustrated in fig. 3.

The interaction of pore and grain boundary is treated theoretically by Nichols [35] and Brook [32] and following their analysis the pore velocity (V_p) is calculated from the relation:

$$V_p = M_p F_p \qquad (10)$$

where M_p is the mobility of the pore and F_p is the force on a pore exerted by an attached boundary. From Nichol's analysis, the driving force, F_p, is given by the relationship:
$F_p = \pi r \gamma_{gb} \sin 2\theta$, where r is the radius of the pore, γ_{gb} the grain boundary energy in MgO and θ the half-angle of a cone having its apex at the pore centre and its base defined by the intersection of the boundary with the pore. The maximum force F_{max} can then be estimated using $\theta = 45°$ and $\gamma_{gb} \simeq \frac{1}{3}\gamma_{SV}$, where γ_{SV} is the solid-vapour surface energy in MgO. Gilman [36] givex $\gamma_{SV} = 1200$ ergs/cm^2 for MgO at room temperature. During calculation, the same value is used at higher temperatures, because the effect of temperature on γ_{SV} is considered negligible when compared to the uncertainties introduced by use of other data. The mobility M_p is estimated from the relation: $M_p = D_p/kT$ and the appropriate mechanism of material transport (e.g., surface diffusion, lattice diffusion or vapour transport) is introduced in D_p throughout its relation with atomic parameters. The pore velocity thus calculated, is then compared with the experimental velocity as shown in table III for transport processes involving surface diffusion, lattice diffusion and vapour transport. It is seen that the experimental data lie, within an order of magnitude, between the velocity calculated for surface diffusion and lattice diffusion mechanisms. The data for the vapour transport mechanism is not in good agreement with the experimental data.

5. Discussion

Entrapment of inert gases during the last stage of sintering has been demonstrated for a number of materials. Deacon *et al* [15], have shown that when polycrystalline compacts of MgO are heated at 1800°C, the trapped gas exhibits a pressure of $\sim$ 1.7 atmospheres for a typical pore size of $\sim$ 10 μm. Bubble formation and gas generation in MgO are also shown to occur from internal sources, possibly due to the presence of OH^-

ions in the crystal [37]. When heated above 1000°C in a reducing atmosphere, certain single crystals of MgO are found to develop cavities with diameters up to $\sim$ 100 μm and gas pressure up to $\sim$ 250 atm. [37]. In the present series of experiments, for the pore sizes involved, the gas pressure is estimated to be in the range of 38 to 68 atm. (assuming that the solubility of gas is negligible in the matrix or in the boundary). The nature of the gas is not identified, but since the specimens are heated in air, some inert gases are expected to be present in the pores. In addition, there may be some trace of chlorine and hydroxyl ions originating from magnesium chloride and the magnesium hydroxide respectively.

During the course of analysis of the results, various theories in the literature were evaluated in order to find an agreement with the data. An analysis of pore migration involving solution [24] and diffusion [10, 14, 32] of gases and vacancy in the matrix or boundary yields results in disagreement with the theoretical prediction. The solution is therefore achieved in terms of random motion of pores in solids. For the pore sizes studied, this seems to be the most likely mode of migration and coalescence of pores as borne out by the literature data of pore sizes in the range of one micron or less [9].

From the data presented in table II it is clear that surface diffusion, lattice diffusion or vapour transport *alone* cannot account for the pore migration in MgO. From the grain size and pore size data presented in fig. 3, it is also clear that an additional contribution to pore migration must come from the dragging of pores by the boundaries. Table III shows that when the pore growth is caused by boundary migration in conjunction with random motion, the experimental data can be adequately described by a combined process involving surface and lattice diffusion mechanisms. In view of the fact that the calculated values give an upper limit of velocities with $F_p = F_{max}$, the agreement is in fact better with surface diffusion as the rate controlling mechanism. Nevertheless, there is an indication in table III, that at higher temperatures, the contribution from lattice diffusion is considerably higher than that from surface diffusion and vice versa at lower temperatures. The vapour transport process appears to compete with the lattice diffusion process only at the highest temperature of measurement (e.g. 1650°C). This is in accord with the theoretical prediction [9] that as the temperature is raised or the pore size increased, lattice diffusion and finally vapour transport become more and more important, assuming two-dimensional random motion of pores.

A further check on the possible rate controlling mechanism can be made by plotting pore velocity against diameter of the pore. Equation 10 gives: $V_p = M_p F_p = (D_p/kT) F_p$, and since F_p is directly proportional to the diameter d, and D_p is proportional to d^{-4} and d^{-3} for surface and lattice diffusion respectively, it follows that $V_p \propto 1/d^3$ for surface diffusion and $V_p \propto 1/d^2$ for lattice diffusion. From a plot of the pore velocity versus diameter as shown in fig. 4, the pooled

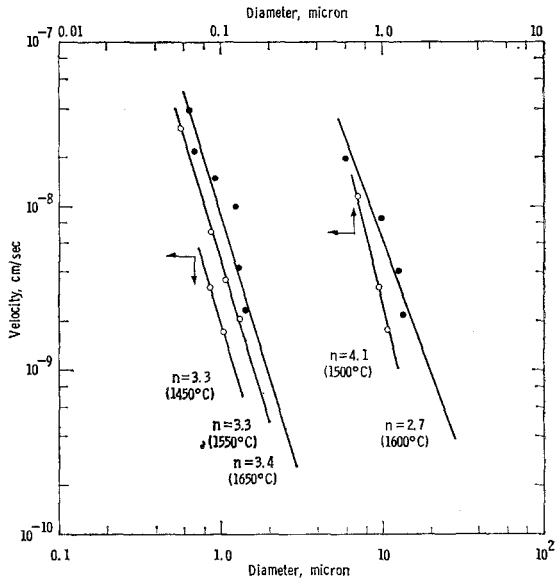

Figure 4 Relation between pore velocity and pore diameter in MgO at various annealing temperatures.

average value of the exponent is estimated to be 3.36 from individual values taken at five temperatures between 1450 and 1650°C. Within the limits of the accuracy of these measurements, the values of the exponents are considered to be in satisfactory agreement with the surface diffusion mechanism. However, it is also possible that minor contributions from other transport mechanisms may be present. Because of the complex process involved in the pore movement as delineated above, similar difficulty is also encountered in interpreting the activation energy as obtained from a plot of pore velocity versus reciprocal absolute temperature. The value of the activation energy thus calculated lies in the range of 48 to 50 kcal/mole. This is less than that

expected for either surface or lattice diffusion of atoms.

6. Conclusion

(1) When polycrystalline compacts of MgO are heated in air, the pores are generated on the plane of grain boundaries, which, on further heat treatment, grow in size and inhibit the normal grain growth in MgO.
(2) Pore growth in MgO cannot be explained by mechanisms involving random two-dimensional motion of pores due to surface diffusion, lattice diffusion or vapour transport of atoms.
(3) Pore growth in MgO can be explained by a mechanism involving pore dragging by boundary migration in combination with a two-dimensional random motion due to surface diffusion. At higher temperatures, contributions from lattice diffusion and vapour transport become increasingly important.

Acknowledgement

The author wishes to thank F. A. Nichols for numerous suggestions during the preparation of this manuscript and B. R. Rossing for a critical review.

References

1. R. S. BARNES and D. J. MAZEY, *Proc. Roy. Soc. A* **275** (1963) 47.
2. R. KELLEY and F. BROWN, *Acta Metallurgica* **13** (1965) 169.
3. E. RUEDL and R. KELLEY, *J. Nuclear Materials* **16** (1965) 89.
4. R. KELLEY and E. RUEDL, *Phys. Stat. Sol.* **13** (1966) 55.
5. R. M. CORNELL and G. K. WILLIAMSON, *J. Nuclear Materials* **17** (1965) 200.
6. MARY E. GULDEN, *ibid* **23** (1967) 30.
7. R. M. CORNELL and G. H. BANNISTER, *Proc. Brit. Cerm. Soc.* No. 7 (February 1967) 355.
8. P. G. SHEWMON, *Trans AIME* **230** (1964) 1134.
9. F. A. NICHOLS, *J. Nuclear Materials* **30** (1969) 143.
10. H. G. BOWDEN and R. W. BALLUFFI, *Phil. Mag.* **19** (1969) 1001.
11. F. N. RHINES, E. BIRCHENALL, and J. HUGHES, *Trans. AIME* **188** (1950) 378.
12. YA. E. GEGUZIN and L. N. PARITSKAYA, *Soviet Powd. Met Metal Ceram.* English Translation (1962) 327.
13. NAYAL A. L. MANSOUR and J. WHITE, *Powder Met.* **12** (1963) 108.
14. T. K. GUPTA and R. L. COBLE, *J. Amer. Ceram. Soc.* **51** (1968) 525.
15. R. F. DEACON, S. F. A. MISKIN, and B. J. LADELL, *Brit. Ceram. Soc.* (1966) 585.
16. F. A. NICHOLS, *Acta Metallurgica* **15** (1967) 365.
17. R. KELLY, *Phys. Stat. Sol.* **21** (1967) 451.
18. E. E. GRUBER, *J. Appl. Phys.* **38** (1967) 243.
19. A. A. CHERNOV, *Sov. Phys. State* **6** (1965) 2240.
20. F. A. NICHOLS, *J. Appl. Phys.* **37** (1966) 2805.
21. W. D. KINGERY and B. FRANCOIS, *J. Amer. Ceram. Soc.* **48** (10) (1966) 546.
22. F. A. NICHOLS, *J. Appl. Phys.* **37** (1966) 4599.
23. G. W. GREENWOOD and A. BOLTAX, *J. Nucl. Materials* **5** (1962) 234.
24. A. WOLFENDEN and K. FARRELL, *ibid* **29** (1969) 133.
25. T. K. GUPTA, *J. Mater. Sci.* **6** (1971) 25-32
26. E. E. UNDERWOOD, A. R. COLCORD, and R. C. WAUGH, in "Ceramic Microstructures" (ed. R. M. Fulrath and J. A. Pask, Proceedings of the Third Berkeley International Materials Conference, June 13-16, 1966)
27. C. S. SMITH and L. GINTHMAN, *Trans AIME* **197** (1953) 81.
28. C. HERRING, in "Structure and Properties of Solid Surfaces" (ed. R. Gomer and C. S. Smith; Univ. of Chicago Press, 1953) 5.
29. W. M. ROBERTSON, "Sintering and Related Phenomena" (ed. G. C. Kuczynski *et al*, Gordon & Breach 1967) 215.
30. R. LINDNER and G. D. PARFITT, *J. Chem. Phys.* **26** (1957) 182.
31. Y. OISHI and W. D. KINGERY, *ibid* **33** (1960) 905.
32. R. J. BROOK. *J, Amer. Ceram. Soc.* **52** (1969) 56.
33. M. S. CHANDRASEKHARAIAH, in "The Characterization of High-Temperature Vapors" (ed. J. L. Margrave, John Wiley & Sons, New York, 1967).
34. E. H. KENNARD, "Kinetic Theory of Gases" (McGraw Hill, New York, 1938).
35. F. A. NICHOLS, *J. Amer. Ceram. Soc.* **51** (1968) 468.
36. J. J. GILMAN, *J. Appl. Phys.* **31** (1960) 2208.
37. A. BRIGGS and D. H. BOWEN, in "Mass Transport in Oxides", (ed. J. B. Wachtman, Jr., and A. D. Franklin, National Bureau of Standards Pub. 296 1968) p. 103.

Received 15 March and accepted 25 March 1971.